Nonlinear dynamics and anisotropic structure of rotating sheared turbulence

A. Salhi, Frank G. Jacobitz, Kai Schneider, Claude Cambon

Nonlinear dynamics and anisotropic structure of rotating sheared turbulence

A. Salhi,[1,2] F. G. Jacobitz,[3,4,*] K. Schneider,[4] and C. Cambon[2]

[1]*Département de Physique, Faculté des Sciences de Tunis, 1060, Tunis, Tunisia*

[2]*Laboratoire de Mécanique des Fluides et d'Acoustique, Ecole Centrale de Lyon, UMR 5509, CNRS, INSA, UCB, 69134 Ecully Cedex, France*

[3]*Mechanical Engineering Department, Shiley-Marcos School of Engineering, University of San Diego, 5998 Alcalá Park, San Diego, California 92110, USA*

[4]*M2P2 - UMR 7340 - CNRS & CMI, Aix-Marseille Université, 38 rue Joliot-Curie, 13451 Marseille Cedex 20, France*

(Received 21 November 2012; revised manuscript received 27 October 2013; published 27 January 2014)

Homogeneous turbulence in rotating shear flows is studied by means of pseudospectral direct numerical simulation and analytical spectral linear theory (SLT). The ratio of the Coriolis parameter to shear rate is varied over a wide range by changing the rotation strength, while a constant moderate shear rate is used to enable significant contributions to the nonlinear interscale energy transfer and to the nonlinear intercomponental redistribution terms. In the destabilized and neutral cases, in the sense of kinetic energy evolution, nonlinearity cannot saturate the growth of the largest scales. It permits the smallest scale to stabilize by a scale-by-scale quasibalance between the nonlinear energy transfer and the dissipation spectrum. In the stabilized cases, the role of rotation is mainly nonlinear, and interacting inertial waves can affect almost all scales as in purely rotating flows. In order to isolate the nonlinear effect of rotation, the two-dimensional manifold with vanishing spanwise wave number is revisited and both two-component spectra and single-point two-dimensional energy components exhibit an important effect of rotation, whereas the SLT as well as the purely two-dimensional nonlinear analysis are unaffected by rotation as stated by the Proudman theorem. The other two-dimensional manifold with vanishing streamwise wave number is analyzed with similar tools because it is essential for any shear flow. Finally, the spectral approach is used to disentangle, in an analytical way, the linear and nonlinear terms in the dynamical equations.

DOI: 10.1103/PhysRevE.89.013020 PACS number(s): 47.27.Ak, 47.27.ek, 47.27.er

I. INTRODUCTION

Turbulent rotating shear flows are important in many different contexts, including engineering, geophysics, and astrophysics. A plane channel flow rotating in the spanwise direction is a well-known example of the interplay of the mean shear with the Coriolis force acting on the turbulence. This results in a dissymmetry of the mean velocity profile and a stabilization or destabilization of the turbulence near the walls, depending on the cyclonic or anticyclonic alignment of the mean shear vorticity and system vorticity [1–3]. Rotating Couette flows [4] and rotating wakes [5,6] exhibit similar effects, with cyclonic and anticyclonic asymmetries. The effects of mean shear combined with rotation or density stratification, but without explicit boundaries, are essential to atmospheric and oceanic flows [7,8]. For more information, see the direct numerical simulation (DNS) study [9] of homogeneous turbulence in stratified shear flow and the references cited therein.

It appears that the most advanced theoretical approach to such flows, applied to the simplest model of spatially uniform mean shear investigated here, is now used in astrophysics for the study of turbulent accretion disks, magnetized or not, with the coupled effects of shear, rotation, and stratification (e.g., [10]). The accretion disk can be seen as a Taylor-Couette flow with circular streamlines and differential rotation $\tilde{\Omega}(r)$. In the local shearing box model [11], the shear rate S results from the differential rotation at a given radial position, so that $S = -[r d\tilde{\Omega}(r)/dr]_{r=r_0}$ and $\Omega = \tilde{\Omega}(r_0)$. Accordingly, the simple model, revisited here, of homogeneous turbulent flow in the presence of a canonical mean flow with constant rates S and Ω, useful for engineering flows, such as the rotating channel studied by Lee *et al.* [12] or an interblades channel in turbomachinery, is now also a model for geophysical and especially astrophysical flows. We will no longer discuss the physical context of the canonical turbulent rotating shear flow, but rather recall the state of the art for the linear and nonlinear approaches to this flow. Our aim here is to extend these analyses, independently of the physical context, considering that the different communities use similar equations but different terminology, with results disseminated in different journals. As far as possible, a secondary goal of this paper is to reconcile such terminologies.

A first approach to understand the effects of the rotation parameter $R_\Omega = -2\Omega/S$ on the dynamics of turbulent rotating shear flow is linear. The rotation parameter R_Ω is defined as the ratio of the Coriolis parameter 2Ω to the shear-induced vorticity $-S$, where Ω is the system rotation and S is the constant shear rate. In addition to the two-component pressureless analyses by Bradshaw [13] and Tritton [14], spectral linear theory (SLT), discussed again in Sec. II, permits a sound analysis, useful for both the mode-by-mode linear stability analysis as well as the prediction of turbulence with a dense spectrum of modes. This analysis focuses on the linear interaction of the mean and fluctuations, neglecting the nonlinear interaction of the fluctuating flow with itself, but the most comprehensive studies [15–17] also solve for the pressure fluctuations. Introduced as "rapid distortion theory" (RDT) by Batchelor and Proudman [18] for irrotational mean flows, SLT was established by Moffatt [19] for the rotational pure shear flow and many subsequent studies followed this approach. We prefer to systematically use the term SLT here instead of RDT because the linkage to RDT is not mentioned in many recent

*jacobitz@sandiego.edu

papers using SLT, and also because the correspondence of "rapid" and "slow" terms with "linear" and "nonlinear" terms is not completely rigorous.

SLT provides the qualitative tendencies for the stabilization or destabilization of turbulence and suggests all the key statistical parameters for exploring the dynamics of two-point statistics. It is performed in spectral space here for mathematical convenience and with a fully anisotropic description. The role of nonlinearity and its subtle interplay with linear operators, however, is far from being understood. It is impossible to assume that the terms of linear and nonlinear origin can be studied separately and modeled in a simple additive way as is often done in single-point closures. The nonlinear effects also do not result in a simple return-to-isotropy trend, and this potential tendency must be considered on a scale-by-scale basis anyway. Possible saturation of the growth of energy and anisotropy in the (linearly) unstable case is another issue. As a third issue, inertial waves induced by rotation can dramatically alter the conventional Kolmogorov cascade, but this effect crucially depends on the R_Ω ratio.

Even if nonlinearity is restricted to the two-dimensional limit, the recent study by Horton *et al.* [20] showed that the angular redistribution of nonlinear perturbations is a universal feature of shear flows, yielding a transverse cascade more complex than the conventional inverse or direct cascades. An investigation of the nonlinear effects of spanwise rotation suggests the consideration of the spectral energy distribution in the two-dimensional manifold $k_3 = 0$. It corresponds to averaging along the spanwise direction in physical space. It is unaffected by rotation in the SLT limit, and even in the nonlinear regime if restricted to purely two-dimensional modes as in [20]. We propose here a fully three-dimensional study so that the nonlinear angular energy drain from $k_3 \neq 0$ to $k_3 = 0$, which is the main feature of "purely" rotating flows, can be recovered (e.g., see [21], chapter 4 and references therein). In this sense, the spanwise two-dimensional manifold is embedded in a fully three-dimensional flow and any effect of rotation, obtained from DNS results here, at $k_3 = 0$ is a typical nonlinear and three-dimensional effect. When rotation is dominant, especially through nonlinear mechanisms, relevant statistical descriptors of the two-dimensional manifold, e.g., $k_3 = 0$, appear directly in physical space, as the tensorial integral length scales with spanwise separation and especially the "two-dimensional energy components" obtained by multiplying them by Reynolds stress components as defined in [15].

More generally, the aim of this paper is to use the most general formalism of two-point statistics for homogeneous strongly anisotropic turbulence in order to disentangle terms from linear and nonlinear dynamics. This qualitative formal approach is presented in Sec. II, while all technicalities are postponed to Sec. V. It is supported, as far as possible, by quantitative results obtained from direct numerical simulation (DNS).

DNS can accurately reproduce the SLT operators, but also include all fully nonlinear terms: advection and pressure redistribution. The pseudospectral DNS approach to fully nonlinear turbulent flows subjected to rotation and shear in a deformed box was first introduced by Rogallo [22]. Comprehensive investigations based on DNS of this flow include the work by Brethouwer [23] and Jacobitz *et al.* [24,25]. While [23] uses a high shear rate to enable a comparison to boundary layer turbulence, the shear rate in [24,25] and the present study is moderate and results in a fully nonlinear evolution of the flow. Previous comparisons of analytical SLT and computational DNS results in Salhi *et al.* [15] were limited to a high shear rate and DNS cases without rotation from [12]. Comparisons with large eddy simulation (LES) results in [15] deal only with single-point quantities and not with the two-point quantities mediated by anisotropic spectra. However, the use of DNS and LES at low shear rate shows large differences with SLT. We wish to emphasize that our study goes beyond a simple comparison between "linear" SLT and "nonlinear" DNS, which was already addressed in previous studies [15,23]. The approach here is mainly spectral, anisotropic, and fully nonlinear.

The paper is organized as follows: The basic theoretical and numerical tools are introduced in Sec. II, including the governing equations and the DNS approach. Section III is devoted to an investigation of the time evolution of turbulent kinetic energy, including the related spherically averaged and one-dimensional spectra as well as their balance equations. The nonlinear effect of rotation on the spanwise two-dimensional manifold is investigated in Sec. IV and similar results for the streamwise two-dimensional manifold are discussed as well. The underlying formalism for disentangling the linear and nonlinear effects is postponed to Sec. V and the structure-based modeling [26] is directly obtained from the decomposition of anisotropy in terms of directional anisotropy and polarization. Finally, conclusions are given in Sec. VI.

II. THEORETICAL AND NUMERICAL TOOLS

A. Spectral linear theory

In homogeneous turbulence subjected to uniform mean velocity gradients and the Coriolis force, there is no velocity scale for the mean field, which is only characterized by a time scale, say S^{-1}. Accordingly, a linearization of the basic equations is not justified by a small ratio of the perturbation velocity with respect to the base flow velocity as in conventional linear stability analysis. It is expected that the nonlinear term in the basic dynamical equations has a typical time scale, say τ_{NL}, significantly larger than the "linear" time scale S^{-1}. Once the nonlinear term is neglected, and often the viscous term for similar reasons, it is possible to solve the linearized inviscid equation for the fluctuating flow, i.e., a Navier-Stokes-type equation with the typical terms arising from the interaction with a mean flow for any initial flow field. The best way is to calculate a deterministic tensorial Green's function once and for all, relating the velocity field at time t to its initial counterpart, possibly a random field. This general solution remains highly complicated in physical space because of the presence of the fluctuating pressure gradient and the nonlocal relationship of the pressure to velocity to maintain zero divergence. Only the use of three-dimensional (3D) Fourier space allows us to derive a tractable linear solution, with pressure obtained in an algebraic way, and a similar treatment of the integro-differential operators involved in the Poisson or Biot-Savart-type equations. In terms of the spectral counterpart $\hat{\boldsymbol{u}}(\boldsymbol{k},t)$ of the velocity fluctuation $\boldsymbol{u}(\boldsymbol{x},t)$,

the linear solution is written as

$$\hat{u}_i(\boldsymbol{k}(t),t) = G_{ij}(\boldsymbol{k},t,t_0)\hat{u}_j(\boldsymbol{k}(t_0),t_0), \quad (1)$$

in which the time dependence of the wave vector $\boldsymbol{k}$ reflects the advection by the mean flow. By forming products of the above equations and applying statistical averaging, denoted by brackets from now on, it is possible to derive statistical correlations of any order in this linear limit. At the second order, as in conventional RDT, the relationship

$$\langle \hat{u}_i^*(\boldsymbol{k}(t),t)\hat{u}_j(\boldsymbol{k}(t),t)\rangle = G_{im}(\boldsymbol{k},t,t_0)G_{jn}(\boldsymbol{k},t,t_0) \times \langle \hat{u}_m^*(\boldsymbol{k}(t_0),t_0)\hat{u}_n(\boldsymbol{k}(t_0),t_0)\rangle \quad (2)$$

gives access to the second-order spectral tensor $\hat{R}_{ij}(\boldsymbol{k}(t),t)$, whose precise definition is recalled in Sec. V [Eqs. (22) and (24)], as expressed in terms of its initial value $\hat{R}_{ij}(\boldsymbol{k}(t_0),t_0)$ via a product of known tensorial Green's functions. Finally, all two-point or single-point second-order statistics are derived from this second-order spectral tensor by weighted integrals over Fourier space. Let us recall first that the Reynolds stress tensor is obtained by integrating the second-order spectral tensor over the whole 3D wave space.

B. Spectral formalism with nonlinear terms

Because our aim is not to simply provide straightforward quantitative comparisons between the results of semianalytical linear SLT and nonlinear DNS, it is useful to introduce the spectral formalism for disentangling the linear and nonlinear terms. As for extracting the purely linear part of these equations, in SLT, the treatment of pressure fluctuations is made via the 3D Fourier transform. This treatment amounts to the solenoidal projection of both linear terms, which are not divergence free, and nonlinear terms. The background fully nonlinear equation to be addressed is

$$\dot{\hat{\boldsymbol{u}}}(\boldsymbol{k},t) + \mathbf{M}(\boldsymbol{k})\hat{\boldsymbol{u}}(\boldsymbol{k},t) + \nu k^2\hat{\boldsymbol{u}}(\boldsymbol{k},t) = -\mathbf{P}\cdot\widehat{(\boldsymbol{\omega}\times\boldsymbol{u})}, \quad \text{with} \quad \boldsymbol{k}\cdot\hat{\boldsymbol{u}} = 0. \quad (3)$$

In this equation, the "overdot" denotes the temporal derivative including the time dependency of the wave vector, $\mathbf{M}$ is the linear matrix which characterizes SLT, $\mathbf{P}$ is the projection operator $P_{ij} = \delta_{ij} - \frac{k_i k_j}{k^2}$, and the nonlinear term is expressed in physical space as the Lamb vector, which is the vector product of the fluctuating vorticity $\boldsymbol{\omega}$ with the fluctuating velocity $\boldsymbol{u}$. In the equation above, this latter term on the right-hand side is both Fourier transformed ("overhat") and projected onto solenoidal space.

From this equation, it is straightforward to extract the equation which governs $\hat{R}_{ij}(\boldsymbol{k},t)$ as

$$\dot{\hat{R}}_{ij}(\boldsymbol{k},t) + M_{in}\hat{R}_{nj} + M_{jn}\hat{R}_{in} + 2\nu k^2\hat{R}_{ij} = T_{ij}(\boldsymbol{k},t), \quad (4)$$

keeping the exact linear terms, only present in SLT with the matrix $\mathbf{M}$, and the viscous terms $2\nu k^2\hat{R}_{ij}$ on the left-hand side. On the right-hand side, the nonlinear term in Eq. (3) gives rise to third-order correlations, which are related to $\langle \hat{\boldsymbol{u}}^* \otimes \widehat{(\boldsymbol{\omega}\times\boldsymbol{u})}\rangle$, gathered as a generalized tensorial transfer term $T_{ij}(\boldsymbol{k},t)$, which also includes nonlinear redistribution terms by pressure. With zero right-hand side, of course, linearized Eqs. (3) and (4) have SLT solutions given by Eqs. (1) and (2), respectively.

From the nonlinear Craya-type equation (4), valid for arbitrary homogeneous anisotropic turbulence, it is possible to derive the corresponding equation for any second-order statistical quantity, two point as well as single point, with an exact separation of the terms originating from SLT, exactly related to $\hat{R}_{ij}$ on the left-hand side, and the terms of nonlinear origin, denoted as T_{ij}. Integration of this equation over the whole Fourier space recovers the governing equation of the Reynolds stress tensor with the "rapid" pressure-strain rate tensor identified on the left-hand side, arising from $\hat{R}_{ij}$, and the "slow" pressure-strain rate tensor on the right-hand side, arising from T_{ij}.

In 3D isotropic turbulence without mean gradient effects, the radial spherically averaged energy spectrum $E(k,t)$, with $k = |\boldsymbol{k}|$, is sufficient for the generation of the spectral tensor and therefore all the second-order statistics. In the same situation, Eq. (4) reduces to a scalar equation for $E(k,t)$, referred to as the Lin equation, which is revisited [Eq. (12)] with the additional shear production term in Sec. III. In fully anisotropic turbulence, more scalars or pseudoscalars are needed to generate $\hat{R}_{ij}(\boldsymbol{k},t)$ and they depend both on the modulus and on the orientation of the wave vector. In the most general case without obvious symmetry, however, simplifications due to the solenoidality and Hermitian symmetry yield a representation of $\hat{R}_{ij}$ by four real pseudoscalars only. The optimal set $[e(\boldsymbol{k},t),\mathcal{H}(\boldsymbol{k},t),Z(\boldsymbol{k},t)]$ of the angle-dependent energy spectrum, angle-dependent helicity spectrum, and polarization term is discussed in detail in Sec. V and more information can be found in [21,27].

Because there is equivalent information in the components of $\hat{R}_{ij}$ and in the the above-mentioned set, Eq. (4) can be replaced by the system of equations governing $(e,Z,\mathcal{H})$, as is done in Sec. V as well. Let us stress that the drastic reduction of the number of generating scalars is not possible for $R_{ij}(\boldsymbol{r},t)$ in physical space because the algebraic expression of solenoidality in Fourier space is essential. The reader is referred to Oughton *et al.* [28] for a study of the same principles and with the seminal references therein [29,30]. The minimal set of generating scalars for general second-rank correlation tensors is extended to magnetohydrodynamics, but the polarization is not clearly extracted and there are no dynamical equations provided. Also note that the structure-based modeling by Kassinos *et al.* [26] can be easily derived from our above-mentioned analyses, as will be discussed in Sec. V.

Important anisotropic statistical indicators are given by the tensorial two-dimensional energy components, or 2DECs, and are addressed in Sec. IV. They characterize a two-dimensional manifold and the distribution of $\hat{R}_{ij}$ at a given wave plane $k_n = 0$, but they are also given in physical space by products of integral length scales with Reynolds stress components. As for any statistical second-order correlation, it is possible to disentangle the linear and nonlinear terms in their dynamics from the weighted spectral integration of Eq. (4).

C. Background dynamical equations, key parameters, and DNS method

We consider homogeneous turbulence subjected to vertical shear with a constant rate S in a frame rotating with constant

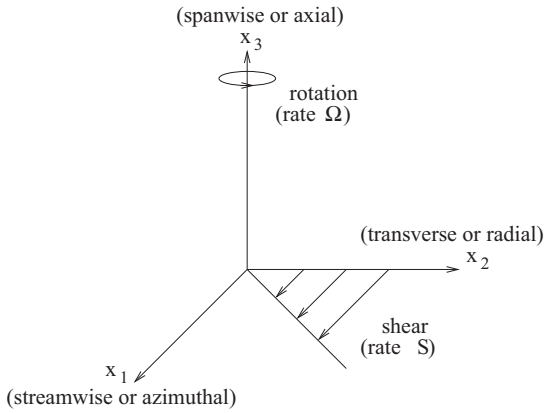

FIG. 1. Schematic of the flow configuration.

rate Ω about the spanwise axis,

$$U_i = A_{ij}x_j = S\delta_{i1}\delta_{j2}x_2, \quad \Omega_i = \Omega\delta_{i3}, \tag{5}$$

as shown schematically in Fig. 1. The Cartesian coordinates $\mathbf{x} = (x_1,x_2,x_3)$ refer to the streamwise, cross-gradient, and spanwise directions, respectively, and δ_{ij} is the Kronecker symbol. The Navier-Stokes equations for the fluctuating velocity field in the rotating frame read

$$\begin{aligned}(\partial_t + u_j\partial_j)u_i + 2\epsilon_{inj}\Omega_n u_j + A_{jm}x_m\partial_j u_i + A_{ij}u_j \\ = -\partial_i p + \nu\partial_{jj}u_i, \quad \partial_i u_i = 0,\end{aligned} \tag{6}$$

in which p denotes the fluctuating pressure divided by a fixed reference density, ν is the kinematic viscosity, $\partial_j(\cdot) = \partial(\cdot)/\partial x_j$, and ϵ_{ijm} is the orientation tensor. The gradient of the Reynolds stress tensor is zero here because of statistical homogeneity. Accordingly, it is not present in Eq. (6) and the mean flow has to be an exact solution of the Euler equations. It follows that the basic absolute vorticity aligns with the spanwise axis, $W_i = -(S - 2\Omega)\delta_{i3}$, and, hence, the rotating shear case with a zero absolute vorticity is characterized by $S - 2\Omega = 0$ or $R_\Omega = -1$. We recall that negative values of R_Ω correspond to the anticyclonic configuration, in which the shear-induced vorticity is antiparallel to the system vorticity and positive values correspond to the cyclonic configuration.

The important parameter for the stability and development of turbulence for this flow is the rotation number $R_\Omega = -2\Omega/S$, which corresponds to the inverse of a typical Rossby number in geophysical applications. Note that our convention is based on the fact that the nonzero component of shear-induced vorticity is $-S$ and not S as in other studies in which the x_2 and x_3 axes are permutated, e.g., [23]. All subsequent relationships in this paper are therefore consistent with these previous studies.

Looking at the shearing-box approximation in astrophysics, stability can be related to a general Rayleigh criterion [31] for rotating shear flows in cylindrical coordinates, as in the limit of a Taylor-Couette flow. The real value of the epicyclic frequency f,

$$\begin{aligned}f^2 = 2\Omega(2\Omega - S), \quad \text{with} \quad f^2 = S^2 B_\Omega, \\ B_\Omega = R_\Omega(1 + R_\Omega),\end{aligned} \tag{7}$$

corresponds to stability, as in the Bradshaw criterion $B_\Omega > 0$ [13,14]. Therefore, the corresponding nomenclature for the directions in Fig. 1 is peripheral or azimuthal (for streamwise), radial (for cross-gradient), and axial (for spanwise). Accordingly, $f^2 = S^2 B_\Omega > 0$ is equivalent to $q < 2$ in astrophysics with an angular velocity $\Omega_r \sim r^{-q}$ in cylindrical coordinates. As an important case, the Keplerian disk is stable, according to these criteria, with $q = 3/2$, $R_\Omega = -4/3$, and $B_\Omega = 4/9 > 0$.

In the direct numerical approach used here to obtain the DNS results, the fully nonlinear equations of motion (6) are solved in a frame of reference moving with the mean flow (see Rogallo [22]) and all dynamically important scales of the velocity field are resolved. This approach allows the application of periodic boundary conditions for $\boldsymbol{X}[= \boldsymbol{x}(t_0)]$ variables in the characteristic lines

$$x_1 = X_1 + \mathrm{St}X_2, \quad x_2 = X_2, \quad x_3 = X_3, \tag{8}$$

equivalent to the mean flow trajectories, and a spectral collocation method is used for the spatial discretization. Seen in 3D Fourier space, the equation solved is essentially the discretized counterpart of Eq. (3). Time advancement is performed with a fourth-order Runge-Kutta scheme. The simulations are carried out on a parallel computer using a grid with $256 \times 256 \times 256$ points. The results analyzed in this study use and extend the direct numerical simulations reported in Jacobitz *et al.* [24] with a large parameter range, $-5 \leqslant R_\Omega \leqslant 5$, including both neutral cases with $R_\Omega = -1$ and $R_\Omega = 0$. The latter delineate the unstable domain centered around $R_\Omega = -1/2$, as well as cyclonic and anticyclonic configurations in the stable regime.

The initial Taylor microscale Reynolds number,

$$\begin{aligned}\mathrm{Re}_\lambda = \frac{q\lambda}{\nu} = 56, \quad \lambda = \left(\frac{5\nu q^2}{\varepsilon}\right)^{1/2}, \\ q^2 = \langle u_i(\boldsymbol{x},t)u_i(\boldsymbol{x},t)\rangle = 2\mathcal{K},\end{aligned} \tag{9}$$

and the initial shear number $S^+ = S\mathcal{K}/\varepsilon = 2$, where $\mathcal{K}$ is the turbulent kinetic energy and $\varepsilon = \nu\langle\partial_j u_i \partial_j u_i\rangle$ is the dissipation rate, are matched in all cases. The Reynolds number reaches values as high as $\mathrm{Re}_\lambda = 120$ and the shear number assumes a value of about $S\mathcal{K}/\epsilon = 6$ in the simulations. Note that in the DNS by Brethouwer [23], the initial S^+ and Re_λ are about 18 and 32, respectively. This stresses our different viewpoint, not to *a priori* favor a comparison of SLT and DNS results, but to place more emphasis on and to further investigate the nonlinear transfer terms and the nonlinear transverse redistribution terms as in [20].

The direct numerical simulations are started from isotropic initial conditions, generated by a separate simulation started from random initial conditions with the following initial energy spectrum (see, also [9,23]):

$$E(K) = C_0 K^2 \exp(-2K/k_p), \tag{10}$$

where C_0 is a normalization constant, $K = |\boldsymbol{K}|$, and $1/k_p$ is a characteristic length scale. In order to let the turbulence develop a significant inertial zone as well as nonlinear transfer, an isotropic precomputation is done for about one eddy-turnover time before applying the mean shear. Accordingly, a more relevant energy spectrum can be chosen as the initial spectrum of isotropic turbulence after this isotropic precomputation.

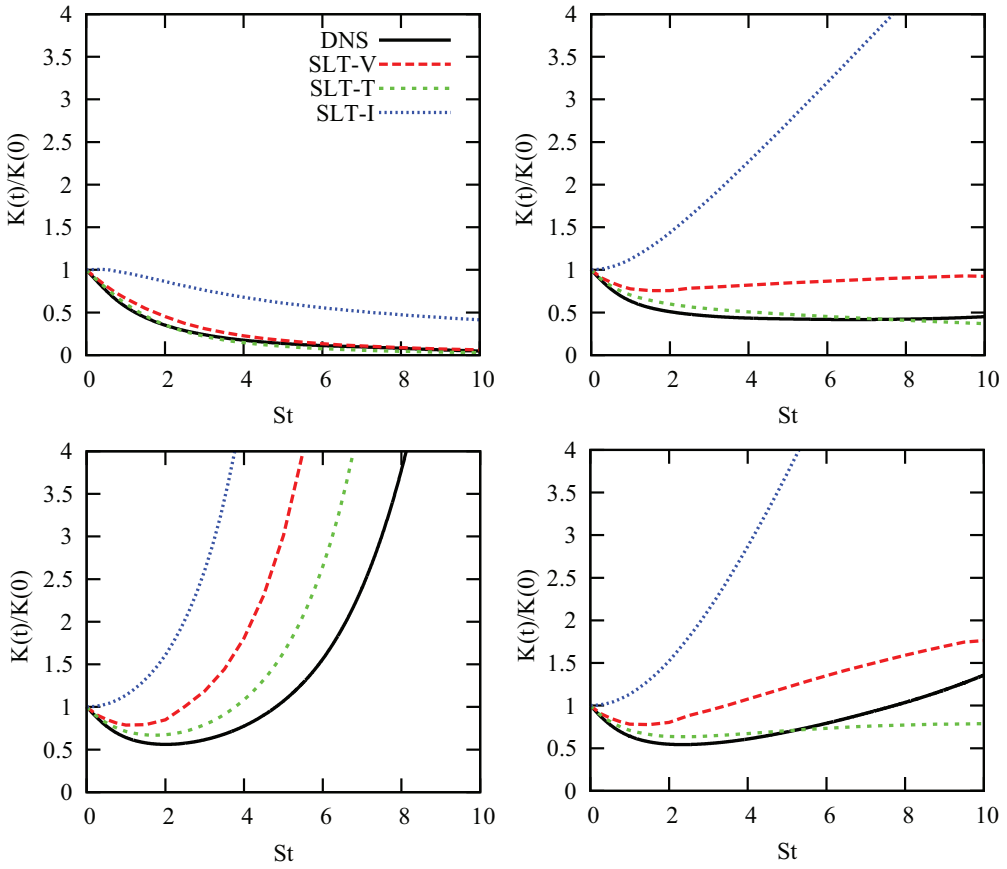

FIG. 2. (Color online) Time history of the turbulent kinetic energy normalized by its initial value for DNS and three versions of SLT: inviscid SLT (SLT-I), viscous SLT (SLT-V), and "Townsend" SLT (SLT-T). Four typical rotation numbers are used: $R_\Omega = -5$ (top left; stable case), $R_\Omega = -1$ (top right; neutral case with zero absolute vorticity), $R_\Omega = -0.5$ (bottom left; most unstable case), and $R_\Omega = 0$ (bottom right; neutral case with pure shear).

III. EVOLUTION OF THE TURBULENCE STATISTICS

A. Time evolution of the kinetic energy

Previous direct numerical simulations with high initial shear rate parameter [23], as well as the present simulations, show that after an initial decay due to viscous effects and a vanishing initial shear production, the turbulent kinetic energy grows with time when the Bradshaw number [in Eq. (7)] is negative or zero, $B_\Omega = R_\Omega\,(1 + R_\Omega) \leqslant 0$, and it continues to decay with time otherwise ($B_\Omega > 0$). In agreement with the Bradshaw criterion, again, the maximum growth rate of the turbulent kinetic energy occurs at $R_\Omega = -0.5$. These results are confirmed in Fig. 2 from DNS and compared to three versions of SLT, inviscid (SLT-I) and viscous SLT. Purely viscous SLT, denoted as SLT-V, uses both the same initial energy spectrum as the DNS and a consistent laminar viscosity. SLT "à la Townsend," denoted as SLT-T, uses an effective initial energy spectrum $E(K) \propto K^4 \exp(-K^2/k_p^2)$ with $S/(\nu k_p^2) = 10$ [15,32], in connection with an implicit effective "turbulent" Reynolds number. The latter version, discussed in detail in [15], does not really incorporate a nonlinear model, but accounts for RDT corrected for decay, with a first implicit model of dissipation fed by nonlinear transfer.

As shown in Fig. 2, the main differences between DNS and SLT results are found for R_Ω values characterizing instability. These differences are due to the fact that the nonlinear interactions between the unstable modes act to reduce the growth rate of the kinetic energy. According to inviscid SLT, when $-1 < R_\Omega < 0$, the modes $k_1 \neq 0$ and $k_3 \neq 0$ undergo a power law growth, while the $k_1 = 0$ mode exhibits an exponential growth with rate $St[(k_3/k)\sqrt{-B_\Omega}]$ (see [16,17]). Because these modes do not interact with each other when the nonlinear terms are neglected, the most unstable mode does not transfer energy to other modes. This mechanism is not altered by viscosity in the absence of nonlinear transfer for feeding of the dissipative scales.

B. Refined analysis: The time development of energy spectra

The definitions of the various spectra are not recalled if they are standard and some details are postponed to Sec. V. The following remark is probably helpful to avoid some possible confusion about fixed or moving wave vectors: In both SLT and DNS, carried out in 3D Fourier space, the characteristic lines (8) or mean trajectories in physical space have an exact counterpart in Fourier space as

$$k_1 = K_1, \;\; k_2(t) = K_2 - St\,K_1, \;\; k_3 = K_3, \qquad (11)$$

so that the wave vector $\boldsymbol{k}(t)$ is time dependent, with $\boldsymbol{K} = (K_1, K_2, K_3) = \boldsymbol{k}(0)$ (e.g., see [19,21,33]). This relationship is not explicitly used in [22] and it is only implicitly ensured by

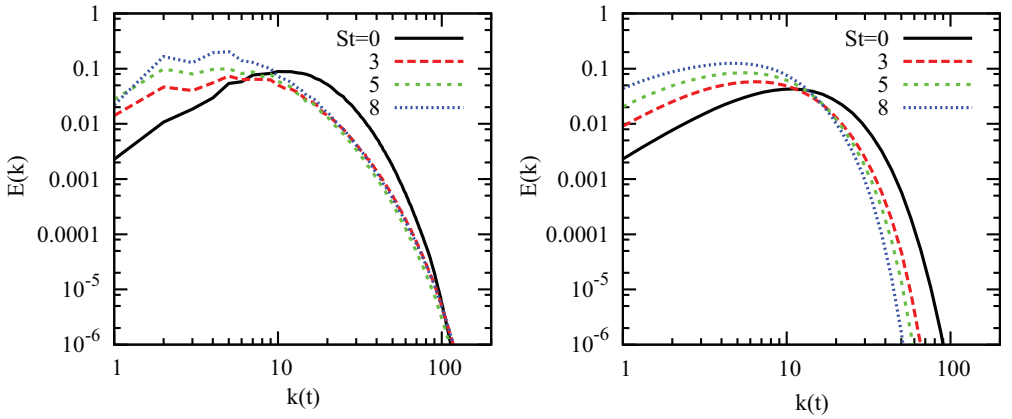

FIG. 3. (Color online) Time development of radial spherically averaged energy spectra in the pure shear case ($R_\Omega = 0$) by DNS (left) and SLT-V (right) for St = 0, 3, 5, 8.

numerics. Of course, if we work at fixed $\boldsymbol{k}$, as often done in the following, this is the initial wave vector $\boldsymbol{k}(-t)$ which must be seen as time dependent [e.g., Eq. (15)].

The transport equation for the radial spherically averaged energy spectrum $E(k)$ reads

$$\frac{\partial E}{\partial t} + T^{(L)}(k) - P(k) + 2\nu k^2 E(k) = T^{NL}(k), \qquad (12)$$

where the terms $T^{(L)}(k)$, $P(k)$, and $T^{NL}(k)$, respectively, denote the radial spectrum of the energy transfer due to the mean advection, the production due to the mean shear, and the nonlinear transfer with zero integral for both the linear and nonlinear energy transfer terms. In DNS, including the present as well as previous simulations related to homogeneous sheared turbulence, the transfer term is computed as the sum of $T^{(L)}(k)$ and $T^{NL}(k)$.

The time development of the radial spectrum $E(k)$ is shown in Fig. 3 at St = 0, St = 3, St = 5, and St = 8 for pure shear flow without rotation ($R_\Omega = 0$). A good agreement is observed in Fig. 3 between the DNS and SLT-V results for the large scales, which are more and more energetic as time elapses. On the other hand, the quasisteadiness of the small scales is only obtained in DNS, after an initial phase of viscous decay (St < 3). This eventual steadiness results from an approximate balance between the nonlinear transfer term $T^{NL}(k)$ in Eq. (12) and the dissipation spectrum $2\nu k^2 E(k)$, as shown in Fig. 4, whereas the production spectrum due to the mean shear is insignificant at these small scales (see also Fig. 6, top right, for $R_\Omega = 0$).

The same conclusions can be drawn when considering the one-dimensional spectrum of the kinetic energy, e.g., the streamwise 1D spectrum $E(k_1)$ in Fig. 5. The continuous decay of the small scales given by SLT-V can be observed in Fig. 5, as compared to their eventual stabilization in DNS.

C. The effect of rotation: Theoretical approach

The effect of rotation is subtle and shown to be very different in the stabilizing, neutral, and destabilizing cases. Without shear, rotation (with angular velocity still along the x_3 direction for consistency but without lack of generality) generates typical waves consistent with zero divergence of the velocity field, called inertial waves, which are characterized by the dispersion frequency

$$\sigma_k = 2\boldsymbol{\Omega} \cdot \frac{\boldsymbol{k}}{k} = 2\Omega \frac{k_3}{k}. \qquad (13)$$

The fact that the system vorticity 2Ω is modulated by a directional parameter linked to the direction of the wave vector, and not its modulus, is essential. Angle variation of the dispersion temporal frequency from 0 to 2Ω is illustrated by "Saint-Andrew cross" structures in experiments and calculations. It allows parametric instabilities, as the elliptical flow instability, to occur and the effect of rotation exactly vanishes at $k_3 = 0$, which corresponds to a two-dimensional manifold by averaging along the spanwise direction in physical space: To say that the zero-frequency (steady) mode of the rotating flow is the two-dimensional mode is equivalent to the Taylor-Proudman theorem.

Another characteristic of the Coriolis force is to produce no energy directly, so that there is no production linked to Ω in the equation for the turbulent kinetic energy or its spectrum. Hence, the effect of rotation must be sought in third-order correlations and, for instance, only explicitly affects $T^{(NL)}$ in Eq. (12). This analysis is consistent with several theoretical and numerical studies (see, e.g., [21], Chap. 4, and references

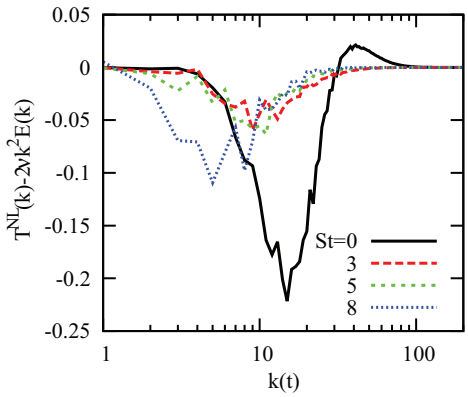

FIG. 4. (Color online) Time development of the transfer term $T^{NL}(k) - 2\nu k^2 E(k)$ for St = 0, 3, 5, 8.

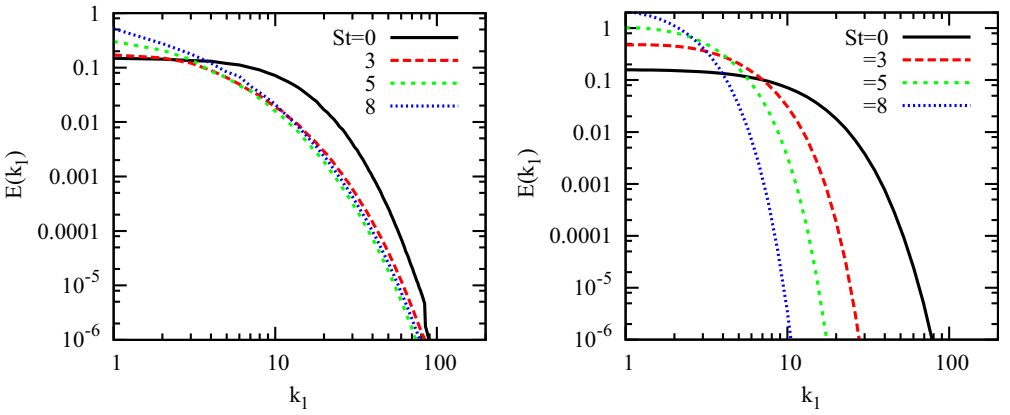

FIG. 5. (Color online) Time development of the streamwise one-dimensional energy spectrum $E(k_1)$ in the pure shear case ($R_\Omega = 0$) for DNS (left) and SLT-V (right).

therein) and was recently confirmed by direct measurements of anisotropic energy transfer [34].

Even though it is possible to build similar nondimensional parameters with S and 2Ω, as the shear rapidity compared to an inverse Rossby number, the dimensional analysis is not very informative if the radically different roles of shear and rotation, separately considered, are not kept in mind. A similar problem arises for the definition of the typical wave numbers for delineating the penetration of anisotropy towards small scales: Similar to the Ozmidov scale in stably stratified turbulence, threshold wave numbers were proposed very early for shear flows (Corrsin [35]) and then for rotating flows (e.g., Zeman [36]) as

$$k_S = \sqrt{\frac{S^3}{\varepsilon}}, \quad k_\Omega = \sqrt{\frac{(2\Omega)^3}{\varepsilon}}, \tag{14}$$

with sometimes slightly different prefactors proposed in previous work, which are of no importance here. Typical values of these parameters are gathered in Table I.

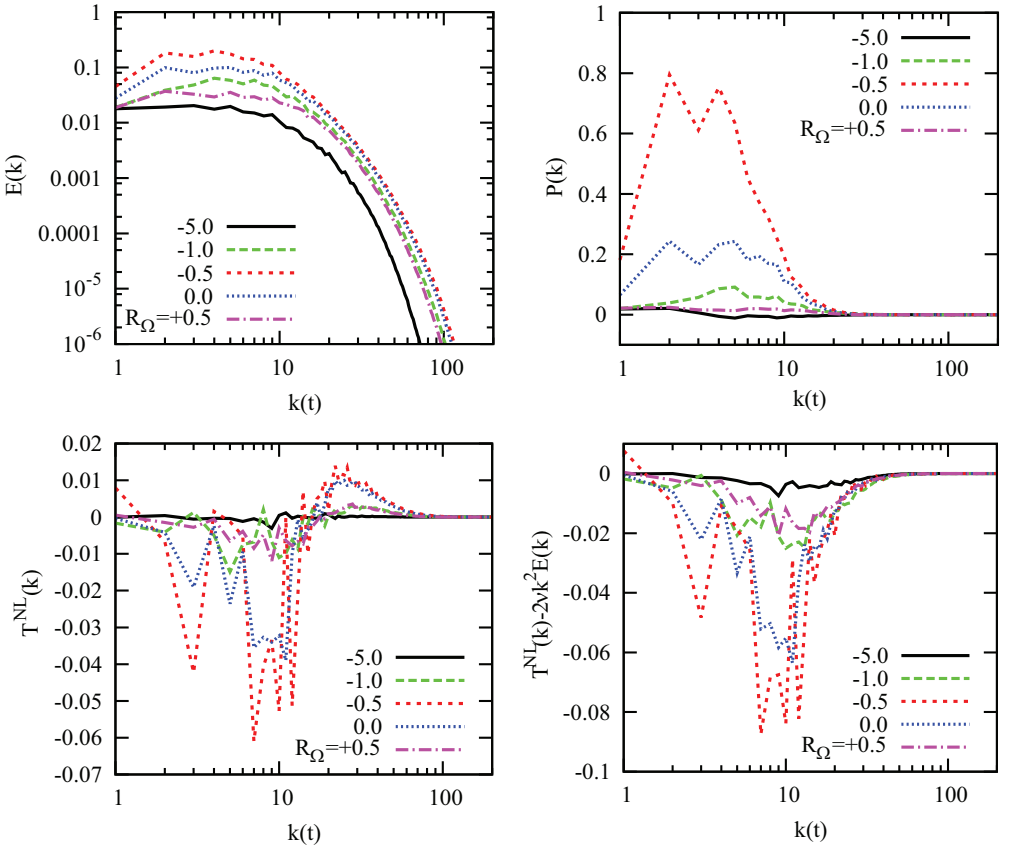

FIG. 6. (Color online) Rotation effects on the radial spectrum of the kinetic energy $E(k)$ (top left), production term $P(k)$ (top right), nonlinear transfer $T^{NL}(k)$ (bottom left), and the difference between the nonlinear transfer term and the viscous term $T^{NL}(k) - 2\nu k^2 E(k)$ (bottom right) at St = 5.

TABLE I. Dissipation rate ε, Corrsin scale $k_S = \sqrt{\frac{S^3}{\varepsilon}}$, and Zeman scale $k_\Omega = \sqrt{\frac{(2\Omega)^3}{\varepsilon}}$ for the DNS data at St = 5 for different values of R_Ω. Note that in all cases $S = 5.60$.

R_Ω	ε	k_S	k_Ω
−10	0.232	27.5	869.7
−5	0.217	28.5	318.3
−1	0.862	14.3	14.3
−0.5	1.660	10.3	3.64
0	1.346	11.4	0.00
+0.5	0.647	16.5	5.83
+1	0.404	20.9	20.9
+5	0.243	26.9	300.6
+10	0.242	27.0	853.0

The effect of the mean shear is to produce turbulent kinetic energy directly and to induce maximum anisotropy at the largest scales by vortex stretching and tilting, until a wave number threshold, such as k_S, is reached with a possible recovery of isotropy for $k > k_S$. Not surprisingly, k_S also appears to be close to the threshold wave number, which separates negative values from positive values of the nonlinear transfer term, as shown in Fig. 4.

Without shear, the effect of rotation is to alter the cascade of energy. Since there is no production, the nonlinear energy transfer is affected by interacting inertial waves, which create anisotropy first in the inertial range of scales. When k_Ω is very large, the anisotropy can increase with k from the largest to the smallest scales as it is shown in the theoretical wave turbulence theory. The large values obtained for k_Ω, much larger than the maximum wave number of the DNS, reflect more the dramatic depletion of ε than the large rotation rate: This depletion of the dissipation is a typical nonlinear effect of rotation, due to the reduction of the energy transfer, which reduces the feeding of the dissipation range.

When rotation is coupled with shear, it is clear that inertial wave dynamics is precluded in all destabilizing and neutral cases, as shown by the epicyclic frequency $\sqrt{2\Omega(2\Omega - S)}$, also equal to $S\sqrt{B_\Omega}$ [Eq. (7)], which becomes imaginary or zero. Only when rotation is dominant, a dispersion frequency close to Eq. (13) is clearly displayed by replacing the system vorticity with the epicyclic frequency. Inertial waves are therefore expected, but always with a direct kinetic energy production, even a weak one, provided that S is not exactly zero.

D. The effect of rotation: DNS results

Considering Fig. 6, it is confirmed that even in the presence of rotation, a clear decoupling arises in terms of the largest and smallest scales: Nonlinearity is responsible for a balance, almost scale to scale, of the positive part of the transfer spectrum with the dissipation spectrum, or $T(k) \sim 2\nu k^2 E(k)$

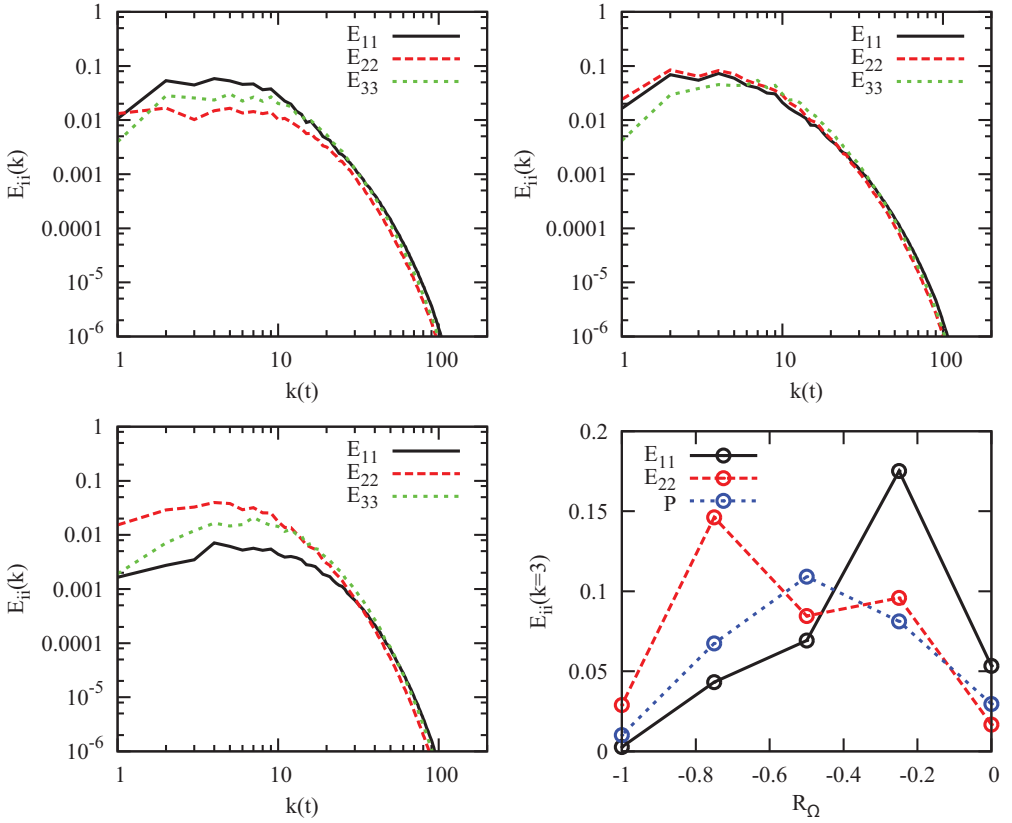

FIG. 7. (Color online) DNS results of the radial spectra of the streamwise, transverse, and spanwise components of the kinetic energy in the pure shear case ($R_\Omega = 0$; top left), in the case with the most destabilizing effect of rotation ($R_\Omega = -0.5$; top right), and in the zero absolute vorticity case ($R_\Omega = -1$; bottom left). The bottom-right panel shows the variation of E_{11}, E_{22}, and P vs R_Ω at large radial scales with $k(t) = 3$ at St = 5.

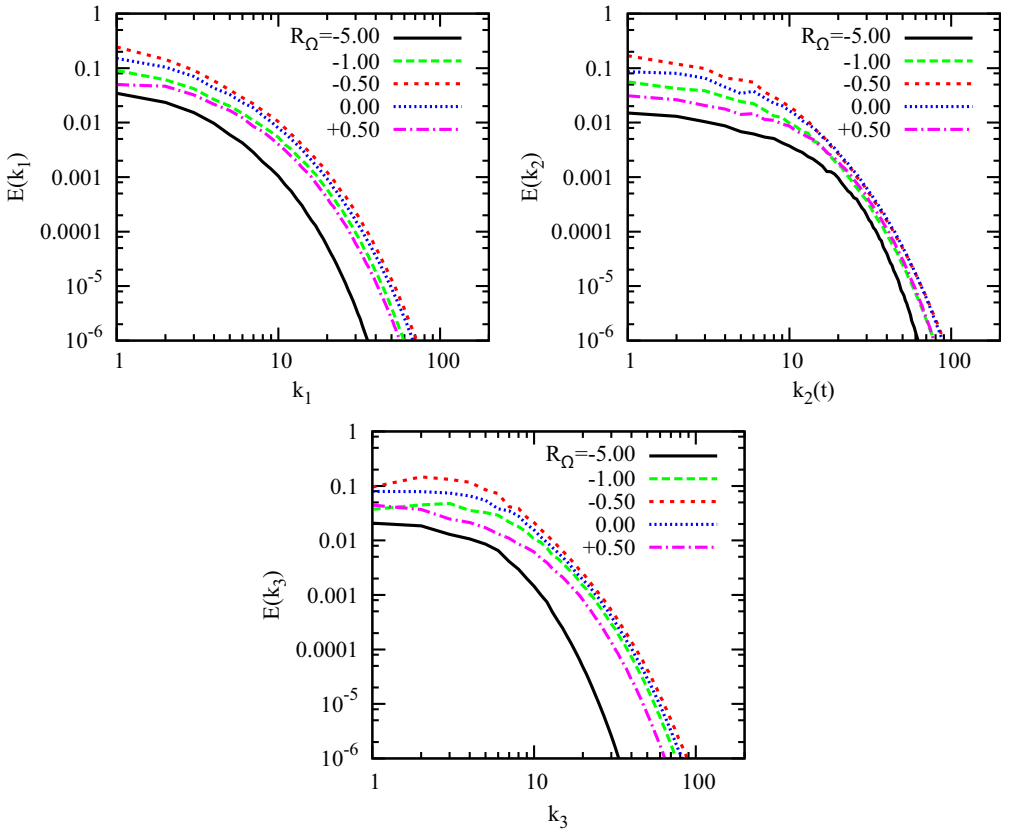

FIG. 8. (Color online) DNS results for one-dimensional energy spectra at $\mathrm{St} = 5$ for different rotation numbers ($R_\Omega = -5, -1, -0.5, 0, +0.5$) for the streamwise component $E(k_1)$ (top left), the cross-gradient component $E(k_2)$ (top right), and the spanwise component $E(k_3)$ (bottom).

if $k > k_*$. The threshold wave number k_S, or k_Ω at moderate rotation rates, remains close to the value k_* for which the spectral transfer changes sign (see Table I). On the other hand, the largest scales remain unsteady, with $\frac{\partial E}{\partial t} \sim P(k) + T(k)$ if $k < k_*$.

In Fig. 7, it is shown how this result depends on the componentiality of the radial spectra, distinguished as streamwise, transverse, and spanwise components. As shown in previous studies (e.g., [12,23]), the dominant contribution to the kinetic energy comes from the streamwise component, i.e., $(1/2)\langle u_1(\boldsymbol{x},t)u_1(\boldsymbol{x},t)\rangle$ in the pure shear flow case. This suggests a study of the spectral components in the presence of rotation in addition to the energy spectra already considered above. Radial spectral components, denoted $E_{ij}(k,t)$ here, are only considered, for the sake of simplicity, at $\mathrm{St} = 5$. They result from spherically averaging the individual components of $\hat{R}_{ij}(\boldsymbol{k},t)$ (see Sec. V). Isotropy, leading to a collapse of the three different components, E_{11}, E_{22}, and E_{33}, is recovered for the largest wave numbers in Fig. 7 (top left and right, and bottom left) after a threshold value close to k_S is reached (see Table I).

Rotation significantly alters, especially at the large scales, the contributions coming from the streamwise and transverse components of the kinetic energy, as illustrated in Fig. 7. To further clarify this point, we have included in Fig. 7 (bottom right) both $E_{11}(k)$ and $E_{22}(k)$ at $k(t) = 3$ versus R_Ω. DNS results reveal that the contribution from $E_{11}(k)$ reaches a maximum at approximately $R_\Omega = -0.25$ and remains more important than the contribution from $E_{22}(k)$ up to $R_\Omega = -0.5$, whereas for $-1 \leqslant R_\Omega < -0.5$, the contribution from $E_{22}(k)$ becomes more important and reaches a maximum at $R_\Omega \approx -0.75$. We note that the production term has a maximum at $R_\Omega = -0.5$.

A second important point is to evaluate the range of scales altered by rotation. Except at $k_3 = 0$, rotation affects all scales, as shown in Fig. 8 (top left), presenting $E(k_1)$ at $\mathrm{St} = 5$ for $R_\Omega = -5, -1, -0.5, 0, +0.5$. This is consistent with the high values of the threshold wave number k_Ω in Eq. (14), at least for the largest rotation rates (see Table I). The figure also reveals that the effect of rotation is approximately the same at all streamwise scales. With respect to the pure shear case, there is an increase of $E(k_1)$ when the rotation effects are destabilizing ($-1 < R_\Omega < 0$) and a decrease when rotation is stabilizing. The pure shear case without rotation ($R_\Omega = 0$) is found to be more energetic than the rotating shear case with zero absolute vorticity ($R_\Omega = -1$), while these two cases are identical according to Bradshaw's stability criterion (i.e., $B_\Omega = 0$). When considering the transverse (or cross-gradient) 1D spectrum, $E(k_2)$, we can see that rotation affects the large scales more than small scales (see Fig. 8, top right), and inversely when considering the spanwise 1D spectrum, $E(k_3)$ (Fig. 8, bottom). Indeed, the Taylor-Proudman theorem states that the effect of rotation vanishes at $k_3 = 0$, but this is valid for the purely linear regime only.

At small radial scales, the contribution to the kinetic energy is due to the transverse k_2 and spanwise k_3 components (see also Fig. 8), while at large radial scales, the contribution from

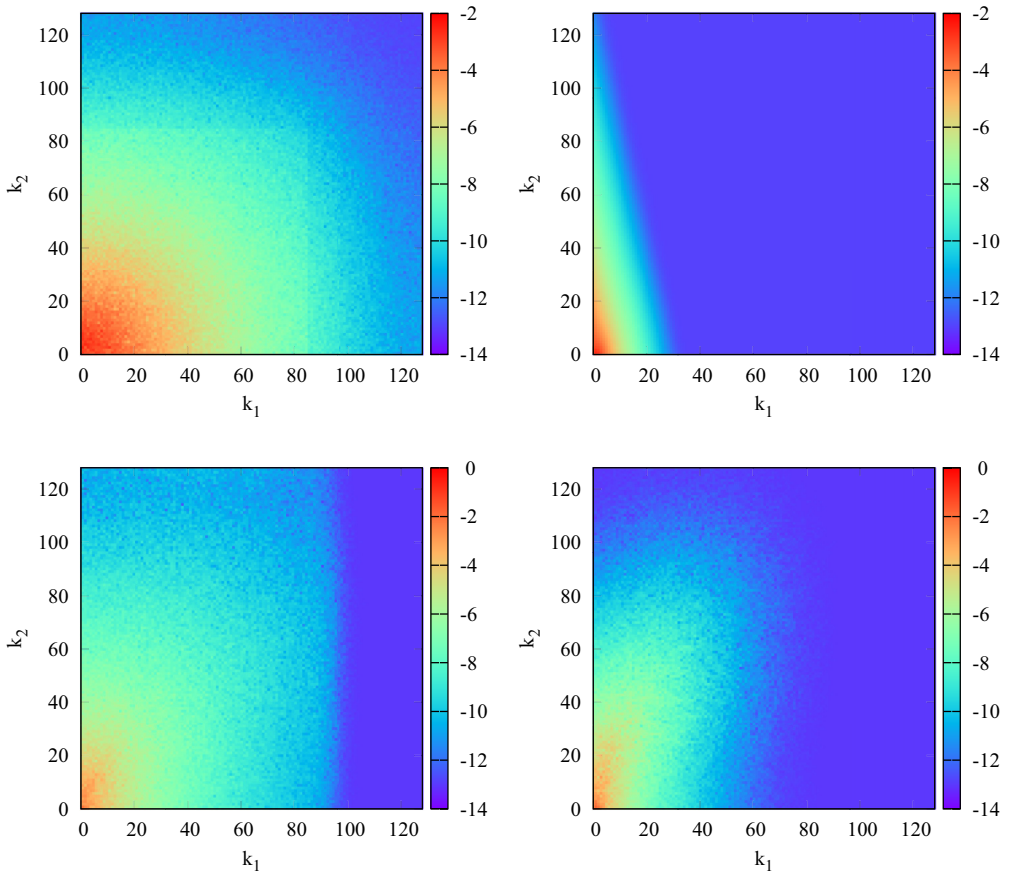

FIG. 9. (Color online) Two-component energy spectrum with $k_3 = 0$ for the initial (isotropic) turbulence from DNS (top left), SLT prediction at St = 5 from Eq. (15) with the DNS initial data (top right), pure shear from DNS at St = 5 (bottom left), and $R_\Omega = +5$ from DNS at St = 5 (bottom right).

the streamwise k_1 component is relatively more important than the contribution of the other two components. At fixed dimensionless time St > 3 and when rotation is destabilizing $-1 < R_\Omega < 0$, the increase of the kinetic energy is mainly due to the increase of the production term, especially at large and intermediate radial scales. At these scales, the difference between the nonlinear transfer term and the viscous term $[T^{NL}(k) - 2\nu k^2 E(k)]$ has a negative sign, as shown in Fig. 6 (bottom right).

To summarize, the evolution of the turbulent kinetic energy in DNS qualitatively compares well with SLT. In particular, SLT-T, à la Townsend, results in a quantitative agreement with DNS for the stable cases with $R_\Omega > 0$ or $R_\Omega < -1$. The unsteadiness of the energy spectrum is mainly determined by the production spectrum at the smallest wave numbers. However, at the largest wave numbers, the time variation of the energy and production spectra tend to vanish as the spectral transfer term equilibrates the dissipation spectrum. The threshold value for the wave number is in fair agreement with the Corrsin scale k_S. A similar analysis was also performed for the streamwise, cross-gradient, and spanwise components of the radial spectra and isotropy is recovered at the largest wave numbers with $k > k_S$. Rotation can affect anisotropy at all scales due to the very large values of k_Ω found in the cases with large rotation rates.

IV. NONLINEAR DYNAMICS IN SPANWISE AND STREAMWISE TWO-DIMENSIONAL MANIFOLDS

Continuing with the effects of rotation, we first consider the two-component energy spectrum $e(k_1,k_2,k_3 = 0,t) = (1/2)\hat{R}_{ii}|_{k_3=0}$ in the spanwise two-dimensional manifold $k_3 = 0$.

Even if noisy, as discussed again in Sec. V, the plots in Fig. 9 reflect the initial isotropy, with quasicircular isolines, and also display the development of anisotropy. A significant alteration by rotation, with respect to the pure shear case, is shown in the case of largest rotation at St = 5. As discussed before, the shape given by SLT is insensitive to rotation, with

$$e(k_1,k_2,k_3 = 0,t) = \frac{E(K)}{8\pi K^2}\left(1 + \frac{K^2}{k^2}\right), \qquad (15)$$

in which $K = \sqrt{k_1^2 + (k_2 + \mathrm{St}k_1)^2}$ (e. g., [21], p. 201). E is the initial radial energy spectrum, determined after the isotropic precomputation.

It is possible to quantify the nonlinear effects of rotation in the spanwise two-dimensional manifold by considering

$$\mathcal{E}_{ii}^{(3)}(t) = 2\pi \int_{-\infty}^{+\infty}\int_{-\infty}^{+\infty} e(\boldsymbol{k},t)|_{k_3=0} dk_1 dk_2, \qquad (16)$$

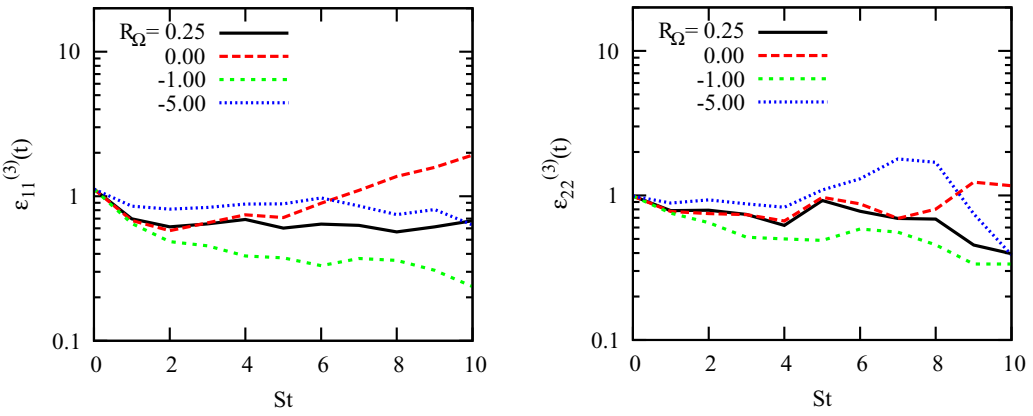

FIG. 10. (Color online) Time evolution of $\mathcal{E}_{11}^{(3)}(t)$ (left) and $\mathcal{E}_{22}^{(3)}(t)$ (right) from DNS with $R_\Omega = 0.25, 0, -1, -5$.

and, more generally, the spanwise two-dimensional energy components (2DECs) for any component $\mathcal{E}_{ij}^{(3)}(t)$.

The most general 2DECs $\mathcal{E}_{ij}^{(n)}(t)$ correspond to the limit $k_n \to 0$ of the one-dimensional spectra, or $E_{ij}(k_n,t)$, which result from integrating the second-order spectral tensor (see Sec. V) in spectral planes normal to k_n. In physical space, the 2DECs are the product of the Reynolds stress component $\langle u_i(\boldsymbol{x},t)u_j(\boldsymbol{x},t)\rangle$ with the associated integral length scale $L_{ij}^{(n)}$ in the x_n direction,

$$\mathcal{E}_{ij}^{(n)}(t) = \langle u_i u_j \rangle L_{ij}^{(n)}, \tag{17}$$

without summation over the indices i and j.

In the inviscid linear limit, the components $\mathcal{E}_{ij}^{(3)}(t)$ are neither affected by the Coriolis force, according to Proudman's theorem, nor by the mean shear [15], but they remain constant and equal to their initial value. The effect of mean shear appears only when viscosity is taken into account in the linear solution. In that case, $\mathcal{E}_{ii}^{(3)}(t)$ (without summation over the index i) decays with time, disregarding the effect of rotation. However, the present DNS results show that $\mathcal{E}_{ii}^{(3)}(t)$ is affected by both rotation and mean shear and that it grows in time for $-1 \leqslant R_\Omega \leqslant 0$. At $k_3 = 0$, the normal component of the pressure-strain contribution vanishes. Hence, the nonlinear transfer term causes the growth of $\mathcal{E}_{33}^{(3)}(t)$, as shown in Fig. 11.

Figures 10 and 11 show that $\mathcal{E}_{33}^{(3)}(t)$ decreases with time and that $\mathcal{E}_{11}^{(3)}(t) + \mathcal{E}_{22}^{(3)}(t)$ increases with time. Hence, the evolution is decoupled for the case with maximum rotation rate. This behavior is consistent with the case of pure (shearless) rotation, as shown in [27,37,38]. The following equations for these quantities display the impact of third-order correlations, reflecting nonlinearity, as

$$\frac{d}{dt}\left(\mathcal{E}_{11}^{(3)} + \mathcal{E}_{22}^{(3)}\right) = \mathcal{D}_\perp^{(3)} + \pi \int_{-\infty}^{+\infty}\int_{-\infty}^{+\infty} (T^{(e)}(\boldsymbol{k},t) + \mathrm{Re}T^{(z)}(\boldsymbol{k},t))|_{k_3=0} dk_1 dk_2, \tag{18}$$

and

$$\frac{d}{dt}\left(\mathcal{E}_{33}^{(3)}\right) = \mathcal{D}_\parallel^{(3)} + \pi \int_{-\infty}^{+\infty}\int_{-\infty}^{+\infty} (T^{(e)}(\boldsymbol{k},t) - \mathrm{Re}T^{(z)}(\boldsymbol{k},t))|_{k_3=0} dk_1 dk_2, \tag{19}$$

in which viscous terms $\mathcal{D}^{(3)}$ are not dynamically active in the "decoupling" of the 2DECs, whereas detailed nonlinear transfer terms for energy, $T^{(e)}$, and for polarization anisotropy, $T^{(Z)}$, discussed again in Sec. V, are essential.

The other important two-dimensional manifold for rotating shear flow corresponds to $k_1 = 0$. The streamwise 2DECs $\mathcal{E}_{ij}^{(1)}$ could thus also be investigated. Townsend [39] pointed out some analytical SLT solutions for these quantities, but only

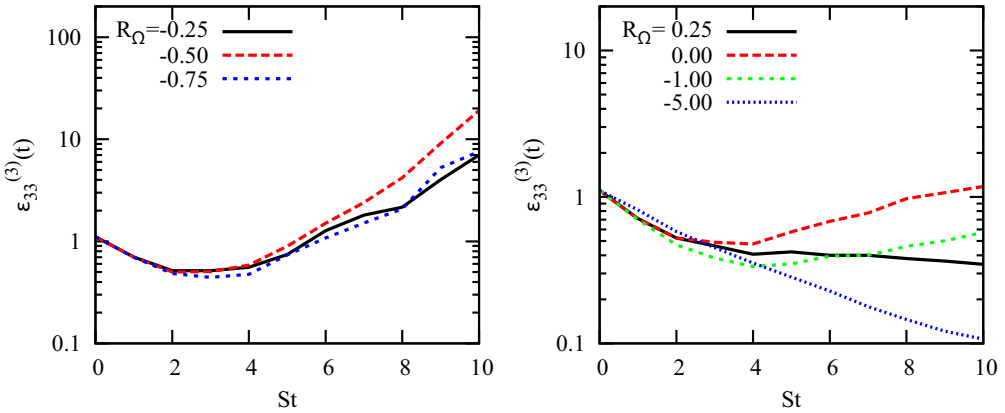

FIG. 11. (Color online) Time evolution of $\mathcal{E}_{33}^{(3)}(t)$ from DNS. Unstable cases with $R_\Omega = -0.75, -0.5, -0.25$ are shown on the left and stable or neutral cases with $R_\Omega = -5, -1, 0, 0.25$ are shown on the right.

for irrotational mean strain. Salhi and Cambon [15] obtained SLT solutions in terms of the Bessel functions for $\mathcal{E}_{ij}^{(1)}(t)$ in the rotating homogeneous shear flow case. A qualitative agreement is found for the fast growth of $\mathcal{E}_{ij}^{(1)}(t)$ between SLT and DNS, whereas very important nonlinear effects are found for the evolution of $\mathcal{E}_{22}^{(1)}$ and $\mathcal{E}_{33}^{(1)}$, the latter being invariant in the inviscid SLT limit without rotation. Corresponding DNS results for all streamwise 2DECs can be supported by governing equations similar to Eqs. (18) and (19), but are not shown here for the sake of brevity.

It can be shown that linear theory cannot predict the time evolution of the spanwise ($k_3 = 0$) 2DECs, and cannot even predict the correct growth of elongation parameters such as $L_{11}^{(1)}/L_{11}^{(3)}$, also obtained from $\mathcal{E}_{11}^{(1)}/\mathcal{E}_{11}^{(3)}$. Even DNS results are not conclusive due to the moderate initial shear rate parameter and the rather short final time, not to mention the finite box effects, if runs are continued over a much larger time. The possible development of streaks, especially in the zero absolute vorticity case with $R_\Omega = -1$, is left for a future study.

To summarize, the 2DECs with a spanwise separation are affected by system rotation and subject to nonlinear evolution, even though they are not affected by system rotation in the linear limit. Hence, there is a significant nonlinear energy transfer from modes $k_3 \neq 0$ to these 2D modes.

V. UNDERLYING FORMALISM FOR ANALYTICALLY DISENTANGLING LINEAR AND NONLINEAR MECHANISMS

A. Full wave vector dependent spectral tensor and nonlinear transfer tensor

In homogeneous isotropic turbulence, all information about the two-point second-order correlations is provided by the radial spectrum $E(k,t)$, whereas information about the two-point third-order correlations derive from $T(k,t)$, denoted as T^{NL} in Eq. (12).

In anisotropic homogeneous turbulence, this information is given by the second-order spectral tensor $\hat{R}_{ij}(\boldsymbol{k},t)$, which is the Fourier transform of the two-point second-order correlation tensor $R_{ij}(\boldsymbol{r},t) = \langle u_i(\boldsymbol{x},t)u_j(\boldsymbol{x}+\boldsymbol{r},t)\rangle$, where $\boldsymbol{r}$ is the vector separating the two points in physical space. An optimal decomposition of the former tensor results from a trace-deviator splitting, restricted to the plane normal to the wave vector, by virtue of incompressibility, or

$$\hat{R}_{ij} = \underbrace{\frac{1}{2}\hat{R}_{nn}}_{e(\boldsymbol{k})} P_{ij} + \underbrace{\mathrm{Re}\left(\hat{R}_{ij} - \frac{1}{2}\hat{R}_{nn}P_{ij}\right)}_{\hat{R}_{ij}^{(\mathrm{pol})}} + \underbrace{\imath\,\mathrm{Im}\left(\hat{R}_{ij} - \frac{1}{2}\hat{R}_{nn}P_{ij}\right)}_{\hat{R}_{ij}^{(\mathrm{hel})}}, \tag{20}$$

in which $P_{ij} = \delta_{ij} - k_i k_j/k^2$ is the dedicated planar projection operator. One thus recovers as the first term the contribution from the trace $e = (1/2)\hat{R}_{nn}$, whereas the deviatoric part consists of a real symmetric tensor $\hat{R}_{ij}^{(\mathrm{pol})}$ and a purely imaginary antisymmetric tensor $\hat{R}_{ij}^{(\mathrm{hel})}$. The first tensor is generated by a single complex-valued scalar $Z(\boldsymbol{k},t)$, called "polarization" (superscript "pol"). The second tensor is generated by a single real helicity spectrum $\mathcal{H}(\boldsymbol{k},t)$, called "helicity" (superscript "hel") [21,40,41]. In order to distinguish the purely 3D isotropic contribution from that of directional anisotropy, the first term can be rewritten as

$$e(\boldsymbol{k},t)P_{ij} = \underbrace{\frac{E(k,t)}{4\pi k^2}P_{ij}(\boldsymbol{k})}_{\hat{R}_{ij}^{(\mathrm{iso})}} + \underbrace{e^{(\mathrm{dir})}(\boldsymbol{k},t)P_{ij}(\boldsymbol{k})}_{\hat{R}_{ij}^{(\mathrm{dir})}}. \tag{21}$$

The terminology "directional anisotropy–polarization anisotropy" is motivated by the analogy between the velocity field in Fourier space $\hat{\boldsymbol{u}}(\boldsymbol{k})$ (normal to the wave vector $\boldsymbol{k}$) and a transversely propagating electromagnetic field (also normal to the wave vector), e.g., directional light or polarized light.

Of course, we consider the theoretical limit of an infinite unbounded flow with full ensemble averaging denoted by the brackets for defining $\hat{R}_{ij}(\boldsymbol{k},t)$ from

$$\hat{R}_{ij}(\boldsymbol{k},t)\delta^3(\boldsymbol{p}-\boldsymbol{k}) = \langle \hat{u}_i^*(\boldsymbol{p},t)\hat{u}_j(\boldsymbol{k},t)\rangle, \tag{22}$$

in which δ^3 is the vectoral Dirac δ distribution and the asterisk denotes the complex conjugate. On the one hand, there is the same amount of information in the spectral tensor and in the second-order two-point correlation tensor in physical space $R_{ij}(\boldsymbol{r},t)$. On the other hand, only the spectral counterpart allows the irreducible decomposition in terms of the minimal set $(e,Z,\mathcal{H})$. Because the spectral tensor is Hermitian positive definite with a zero eigenvalue along the direction of $\boldsymbol{k}$, which is the geometric solenoidal constraint, it is of rank 2 and its two nonzero positive eigenvalues are

$$\langle s_1^2\rangle = e + \sqrt{|Z|^2 + \mathcal{H}^2} \quad \text{and}$$
$$\langle s_2^2\rangle = e - \sqrt{|Z|^2 + \mathcal{H}^2}. \tag{23}$$

The formulas for extracting separately Z and $\mathcal{H}$ from $\hat{R}_{ij}(\boldsymbol{k},t)$ in Eq. (20) are given in [27,40].

How can DNS provide access to these quantities? This question is often eluded in quasi-isotropic flows. In the periodic domain, the wave vector is discretized as $k_i = n_i 2\pi/\ell_0$, with n_i a relative integer, so that the spectral tensor is approached by

$$\hat{R}_{ij}(\boldsymbol{k}) = \left(\frac{\ell_0}{2\pi}\right)^3 \langle \hat{u}_i^*(\boldsymbol{k})\hat{u}_j(\boldsymbol{k})\rangle. \tag{24}$$

Before using the conventional nondimensional form of the box length $\ell_0 = 2\pi$, the above equation illustrates the correct limit of the Dirac term $\delta^3(\boldsymbol{p}-\boldsymbol{k})$ for the continuous case in Eq. (22). Since the direct numerical simulations are started from a single realization of the initial velocity field, as is the customary practice, there is no ensemble averaging, and only the dyadic unaveraged realization of $\hat{R}_{ij} \sim \hat{u}_i^*\hat{u}_j$ is available. In this case, the dyadic tensor is of rank 1 and has only a single nonzero eigenvalue $s_1^2 = 2e = \hat{u}_i^*\hat{u}_i$, so that $s_2^2 = e - \sqrt{|Z|^2 + \mathcal{H}^2} = 0$, and separate information on $e,Z,\mathcal{H}$ cannot be disentangled.

Accordingly, a surrogate of ensemble averaging, denoted here by brackets, is needed to reproduce the full spectral tensor with its two distinct nonzero eigenvalues, equivalent to the $(e,Z,\mathcal{H})$ set. In forced turbulence, time averaging can be used because stationarity can be assumed for statistics. However,

this is not possible in our case of nonstationary turbulence, so that we have no access to the complete set $(e,Z,\mathcal{H})$ from our DNS. Fortunately, space-averaged quantities, which correspond to averaging the full spectral tensor over bins of wave vectors, can be considered as statistical, ensemble averaged quantities, assuming some ergodicity. For instance, the 3D energy spectrum $e(\boldsymbol{k},t) \sim \hat{u}_i^* \hat{u}_i$ is not obtained as a true statistical quantity, but spectra computed from $\hat{u}_i^* \hat{u}_i$ as plane averages $E(k_i,t)$ or as spherical averages $E(k,t)$ are statistical quantities.

Now let us go back to our dynamical problem of disentangling the linear and nonlinear terms, considering only the theoretical homogeneous context with continuous wave vectors. From Eq. (3) for $\hat{\boldsymbol{u}}$, using Eq. (22), the Eq. (4) for $\hat{R}_{ij}$ is easily determined, in which the pressure is exactly determined via an algebraic solenoidal projection of both the linear and nonlinear terms. This equation for $\hat{R}_{ij}$ is strictly the equivalent to a set of three equations, in terms of $(e,Z,\mathcal{H})$, using the irreducible form from Eq. (20), so that Lin's equation in isotropic turbulence is generalized as

$$\dot{e} + 2\nu k^2 e + \underbrace{\frac{\dot{k}}{k} e + \mathrm{Re}\left(Z \left[\frac{\dot{k}}{k} + \imath S \frac{k_3}{k} \right] \right)}_{\text{explicit SLT part for } e} = T^{(e)}(\boldsymbol{k},t), \quad (25)$$

$$\dot{Z} + 2\nu k^2 Z + \underbrace{\frac{\dot{k}}{k} Z + e \left[\frac{\dot{k}}{k} - \imath S \frac{k_3}{k} \right] + 2\imath Z \left[(2\Omega + S/2) \frac{k_3}{k} \right]}_{\text{explicit SLT part for } Z} = T^{(Z)}(\boldsymbol{k},t), \quad (26)$$

$$\dot{\mathcal{H}} + 2\nu k^2 \mathcal{H}(\boldsymbol{k},t) = T^{(\mathcal{H})}(\boldsymbol{k},t). \quad (27)$$

These equations are given in [27] for any mean velocity gradient matrix A_{ij} and for any system vorticity. In the present case of pure plane mean shear with spanwise rotation, their simplest form, given above, is found for the polar axis of the polar-spherical frame of reference for $\boldsymbol{k}$ chosen along the cross-gradient direction. In addition to the classical dissipation terms and the time-derivative terms, i.e., the "overdot" denotes the time derivative at fixed $\boldsymbol{k}$ following the characteristic lines of Eq. (11), other exact linear terms in these equations display two angle-dependent coefficients:

$$\frac{\dot{k}}{k} = -S \frac{k_1 k_2}{k^2}, \quad \text{and} \quad S \frac{k_3}{k},$$

in addition to the classical dispersion relation of inertial waves, $2\Omega k_3/k$, which explicitly affects the polarization deviator only.

Note that the e equation is also used in [20], but only in the enforced 2D case with $k_3 = 0$. The use of compact disturbances as cyclonic (with respect to the mean shear vorticity) or anticyclonic vortices is very informative for transient growth and bypass transition in connection with transverse cascades.

From the general decomposition of the spectral tensor, it is possible to derive a threefold splitting of any second-order statistical quantity, either two point or single point. Note that the contribution from the helicity spectrum vanishes for any subsequent statistical quantity investigated here, by summing up $\boldsymbol{k}$ and $-\boldsymbol{k}$ contributions. Therefore, this helical contribution will not be considered here, except in the following remark.

The helicity spectrum in the theoretical continuous case is given by

$$\tfrac{1}{2} \langle \widehat{\boldsymbol{\omega}}_i^*(\boldsymbol{p}) \hat{u}_j(\boldsymbol{k}) \rangle = k \mathcal{H}(\boldsymbol{k}) \delta^3(\boldsymbol{k} - \boldsymbol{p}), \quad (28)$$

so that the single-point statistical helicity is

$$\frac{1}{2} \langle \boldsymbol{\omega} \cdot \boldsymbol{u} \rangle = \int_{-\infty}^{+\infty} \int_{-\infty}^{+\infty} \int_{-\infty}^{+\infty} k \mathcal{H}(\boldsymbol{k}) d^3\boldsymbol{k},$$

and a radial helicity spectrum $H(k)$ could be defined by spherically averaging $k\mathcal{H}(\boldsymbol{k})$, so that $\frac{1}{2}\langle \boldsymbol{\omega} \cdot \boldsymbol{u} \rangle = \int_0^\infty H(k) dk$. One recovers the same relationship as for the kinetic energy when passing from $e(\boldsymbol{k})$ to $E(k)$ and to $(1/2)\langle u_i u_i \rangle$. In addition, Eq. (27) shows immediately that the spectrum of "superhelicity" is $k^3 \mathcal{H}(\boldsymbol{k})$. Of course, $k\mathcal{H}(\boldsymbol{k})$ contains much more information than the single-point helicity correlation because there is a bijection between this spectral scalar and the two-point correlation scalar in physical space $\langle \boldsymbol{\omega}(\boldsymbol{x}) \cdot \boldsymbol{u}(\boldsymbol{x} + \boldsymbol{r}) \rangle$.

From the $\mathcal{H}$ equation, it is deduced that the mean flow cannot produce any helicity spectrum, in agreement with a remark by Lumley for a mean flow with a center of symmetry. Such a spectrum must be initialized or forced to be present. On the other hand, local helicity is present on particular realizations of the flow, as previously investigated (see, e.g., [25,42,43]). In order to initialize a nonzero helicity spectrum, using the $e,Z,\mathcal{H}$ formalism, it is important to note that the initial anisotropy and the initial helicity may fulfill mutual constraints, in agreement with the realizability condition $[\langle s_2^2 \rangle \geqslant 0$ from Eq. (23)]. On the other hand, the dynamical coupling of the helicity spectrum, once initialized, with other e and Z terms is essentially nonlinear, mediated by the generalized transfer terms $T^{(e,Z,\mathcal{H})}$.

Is there a hope of producing helicity from a physical process, and not from the artificial initialization or forcing, in a purely homogeneous flow? A positive answer can be given in the case of stably stratified buoyant turbulence, even better with rotation, and even without shear [44]. With the notations used here, the possible net production of the helicity spectrum results from its linear coupling with the poloidal-toroidal cross correlation (or the imaginary part of Z, also connected with "stropholysis" [26]), and the toroidal flux of buoyancy.

B. Spectral quantities and single-point tensors

Any averaged spectral quantity and single-point tensor can be expressed as a sum of three contributions, i.e., isotropic, directional, and polarization, by integrating Eqs. (20) and (21) with dedicated weighting coefficients in Fourier space. In addition, the exact integrands can be derived for all the terms present in their governing equations, in terms of e, Z, $T^{(e)}$, and $T^{(z)}$ using Eqs. (25) and (26). For instance, the spanwise 2DECs in Eqs. (18) and (19) correspond to a planar integration at $k_3 = 0$ of $e \pm Z$, so that their evolution is dependent on the nonlinear transfer terms $T^{(e)} \pm T^{(z)}$.

As a last application, the structure-based tensors [26] are easily recovered from our general threefold decomposition as

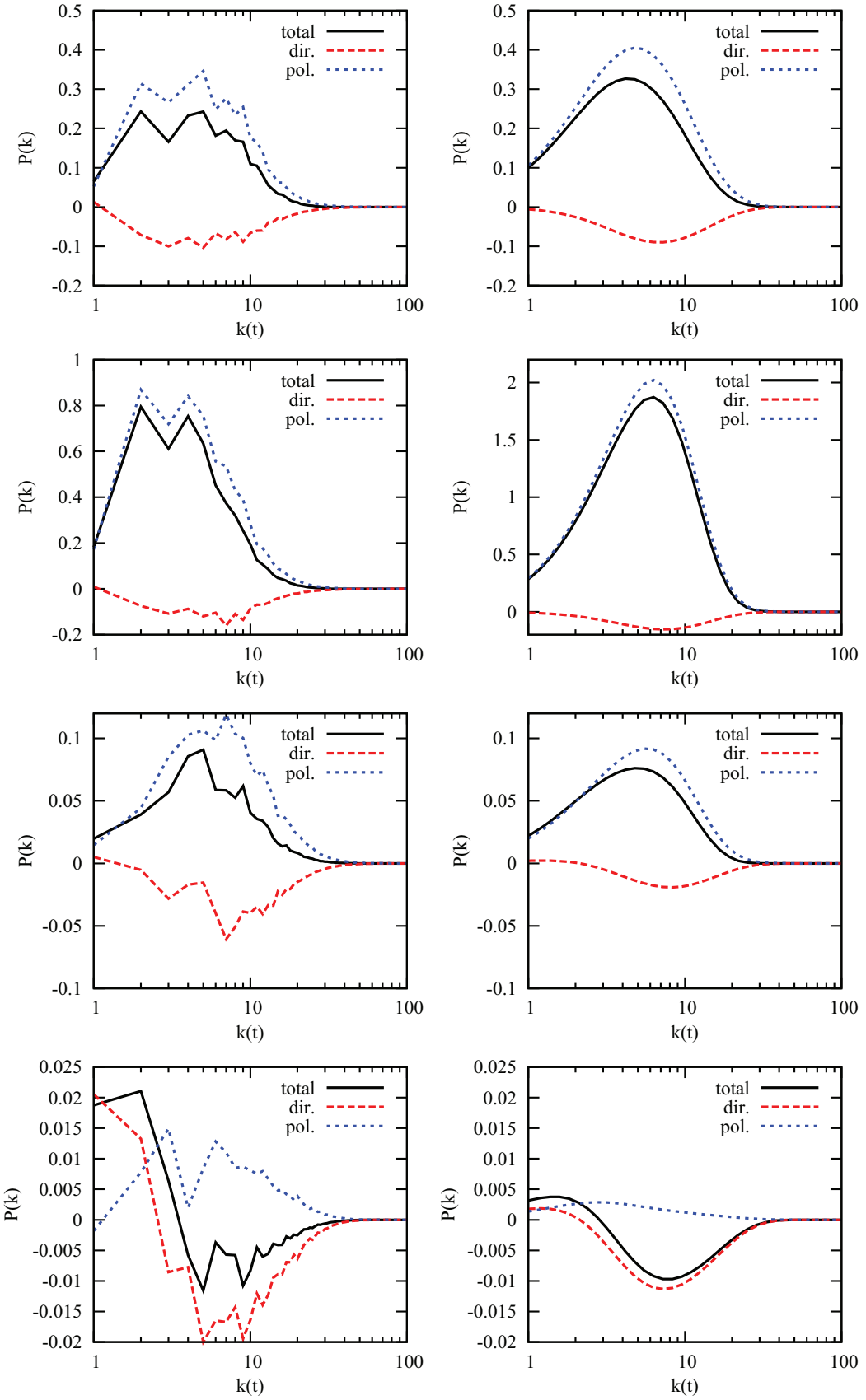

FIG. 12. (Color online) Radial spectra of the production $P(k)$ and the parts $P^{(e)}(k)$ (dir.) and $P^{(z)}(k)$ (pol.) at St $= 5$. DNS results (left) and SLT-V results (right) are compared. R_Ω is varied from top to bottom: $R_\Omega = 0$ (pure shear case), $R_\Omega = -0.5$ (most unstable rotating shear case), $R_\Omega = -1$ (zero absolute vorticity case), $R_\Omega = -5$ (a stabilized rotating shear case).

follows:

$$\langle u_i u_j \rangle = 2\mathcal{K}\left(\frac{1}{3}\delta_{ij} + b_{ij}^{(\mathrm{dir})} + b_{ij}^{(\mathrm{pol})}\right), \tag{29}$$

$$D_{ij} = 2\mathcal{K}\left(\frac{1}{3}\delta_{ij} - 2b_{ij}^{(\mathrm{dir})} + 0\right), \tag{30}$$

$$C_{ij} = 2\mathcal{K}\left(\frac{1}{3}\delta_{ij} + b_{ij}^{(\mathrm{dir})} - b_{ij}^{(\mathrm{pol})}\right). \tag{31}$$

As a consequence, the deviatoric part of the Reynolds stress tensor appears as a sum of two contributions from different origins,

$$b_{ij} = b_{ij}^{(\mathrm{dir})} + b_{ij}^{(\mathrm{pol})},$$

with the first term carrying the same anisotropic information as the "dimensionality tensor" D_{ij}. One recovers the fact that the "circulicity tensor" C_{ij} is not independent of the others.

Previous observations of the separate behaviors of $b_{ij}^{(\mathrm{dir})}$ and $b_{ij}^{(\mathrm{pol})}$ can be summarized as follows. Kassinos *et al.* [26] suggested that for flows dominated by irrotational strain, "dimensionality" is equal to "componentality," which means with our notations $-2b_{ij}^{(\mathrm{dir})} = b_{ij}$ or

$$b_{ij}^{(\mathrm{dir})} = -\tfrac{1}{2}b_{ij}; \quad b_{ij}^{(\mathrm{pol})} = \tfrac{3}{2}b_{ij}. \tag{32}$$

This result was shown to be a generic SLT result for isotropic initial data, for any mean flow, rotational or not, but for very short time (shorter than the expected time of relevance of RDT) in [21,41]. A second point was the trend to damp $b_{ij}^{(\mathrm{pol})}$ by a dominant rotation via the linear phase mixing of inertial waves in the case of initial anisotropy [45]. A third point is the creation of a mildly positive value of the component of $b_{33}^{(\mathrm{dir})}$ along the rotation axis via a nonlinear effect of rotation yielding saturated two dimensionalization [38,46]. The saturation of the two-dimensional trend was quantified by an asymptotic value, $b_{ij}^{(\mathrm{dir})}\frac{\Omega_i\Omega_j}{\Omega^2} \sim 0.08$, much smaller than the theoretical value in a purely 2D flow, $b_{ij}^{(\mathrm{dir})}\frac{\Omega_i\Omega_j}{\Omega^2} = 1/6$, or, equivalently, $D_{ij}\frac{\Omega_i\Omega_j}{\Omega^2} = 0$.

It is therefore possible to disentangle the contributions from directional anisotropy and the contribution from polarization anisotropy for the production term in the equation for the turbulent kinetic energy by considering the component b_{12} and using its splitting in Eq. (29). Results, found to be very consistent between DNS and SLT-V, are not shown here for the sake of brevity and because more informative results are given on the related spectra in Fig. 12. The relationship in Eq. (32) is roughly valid for the neutral cases, but less so for the most unstable case, in which the anisotropy results essentially from the polarization term, and not at all in the stabilized case. For the latter case, the anisotropy results essentially from the directional part, in agreement with a "rapid" damping of the polarization part by significant rotation. These results illustrate structure-based modeling, using the equivalent relationship in Eq. (32), but applied to the extra-diagonal component related to the production term.

Some observed trends can be explained by the structure of the linear e/Z coupling in Eqs. (25) and (26). Rotation first affects the polarization via the imaginary term in Eq. (26). The only exception is the zero tilting vorticity, which vanishes for $R_\Omega = -1/2$, and yields maximum destabilization together with maximum polarization anisotropy. In a second step, Z is created and can then linearly alter the e equation via the Z term in Eq. (25). Finally, all effects can be coupled by the nonlinear transfer terms, which are only accounted for in DNS.

In summary, any statistical quantity can be split into contributions that are purely isotropic, originate from directional anisotropy, and originate from polarization anisotropy. For example, this decomposition gives access to the spectrum of both parts of the component $b_{12} = b_{12}^{(\mathrm{dir})} + b_{12}^{(\mathrm{pol})}$. Also, the decomposition in terms of the directional anisotropy and polarization anisotropy corresponds directly to the structure-based tensors introduced in [26].

VI. CONCLUSION

Turbulent shear flow with rotation around the spanwise direction is a well-studied generic flow case. However, former studies mainly emphasized the linear SLT-relevant regime for comparison to DNS results. In this paper, due to the choice of initial conditions, there is no dominance of linear effects, even at moderate times, so that the nonlinear terms always remain significant.

As in previous studies, e.g., [15], the development of the turbulent kinetic energy in DNS qualitatively compares well with SLT. SLT refinements including viscous or effective decay, particularly for SLT-T, à la Townsend, yield quantitative agreement for the stable cases with $R_\Omega > 0$ or $R_\Omega < -1$.

This energy analysis is rounded off with a consideration of the radial energy spectrum, obtained by spherical averaging, and the related spectral terms in its budget. A spectral separation between large and small wave numbers k is found. The time variation of the energy spectrum is almost entirely governed by the production spectrum at the smallest wave numbers, e.g., $k \sim 20$ in Figs. 3 and 6, whereas both unsteadiness for the energy and production tend to vanish as the spectral transfer term tends to equilibrate the dissipation spectrum at the largest wave numbers, e.g., Fig. 4. The threshold value of the wave number is in fair agreement with the Corrsin scale k_S [see Eq. (14) and Table I]. This scale-by-scale analysis was also performed for the "componental" anisotropy, looking at the radial spectra of the streamwise, cross-gradient, and spanwise Reynolds stress components. As shown in Fig. 7, isotropy is recovered at the largest wave numbers, again after a threshold value close to k_S is reached. On the other hand, rotation can affect the anisotropy at all scales and this finding is consistent with the very large values of k_Ω [Eq. (14) and Table I] found in the cases with large rotation rates.

The one-dimensional spectra of the kinetic energy, integrated over planes, provide additional information, as shown in Figs. 5 and 8. These spectra display, in the limit $k_n \to 0$, informative quantities, called the two-dimensional energy components (2DECs), which are equivalent to the products of integral length scales with the related Reynolds stress components.

The 2DECs with a spanwise separation are affected by the system rotation and subject to a nonlinear evolution, even if they are constant in the inviscid linear limit. Note that

$k_3 = 0$ corresponds to the two-dimensional manifold related to the spanwise direction, which is not affected by the system rotation in the linear limit. Accordingly, the dependence of R_Ω for these quantities reflects a significant nonlinear energy transfer from modes $k_3 \neq 0$ to these 2D modes. Consequently, SLT gives no relevant information for these quantities, from two-component energy distributions in Fig. 9 to 2DECs with a spanwise separation, and one partly recovers by DNS the nonlinear dynamical decoupling of $\mathcal{E}_{33}^{(3)}$ from $\mathcal{E}_{11}^{(3)} + \mathcal{E}_{22}^{(3)}$, which characterizes pure rotation.

Any statistical quantity can be split into a purely isotropic part, a contribution from directional anisotropy, and a contribution from polarization anisotropy. This is applied to the spherically averaged production spectrum, which is split into a directional part and a polarization part. This decomposition gives access to the k spectrum of both parts of the component, $b_{12} = b_{12}^{(\mathrm{dir})} + b_{12}^{(\mathrm{pol})}$, involved in the kinetic energy production of the deviatoric tensor. The exact correspondence of this decomposition in terms of the directional anisotropy and polarization anisotropy with structure-based tensors introduced in [26] is recalled in Sec. V for the sake of completeness.

For perspectives beyond the plane shear flows or a generalization to nonhomogeneous flow cases, a similar stability analysis of rotating two-dimensional flows to three-dimensional disturbances can be generalized to hyperbolical and elliptical flows, using the improved SLT approach [47], and this can be extended to nonhomogeneous flows using the Wentzel-Kramer-Brillouin (WKB) SLT formalism [48]. In addition, a zonal analysis of the rotating channel flow could be performed in connection with the formation of streaks in a central zone, where zero absolute vorticity ($R_\Omega = -1$) is almost recovered.

ACKNOWLEDGMENTS

F.G.J. acknowledges the support from an International Opportunity Grant from the University of San Diego and the hospitality at the Laboratoire de Mécanique, Modélisation & Procédés Propres (M2P2) in Marseille. A.S. acknowledges the hospitality at LMFA in Lyon and at M2P2 in Marseille. K.S. acknowledges the financial support from the ANR project SiCoMHD and the hospitality at the University of San Diego. C.C. acknowledges the support from the ANR Contract No. 08-BLAN-0076 "ANISO."

[1] J. P. Johnston, R. M. Halleen, and D. K. Lezius, J. Fluid Mech. **56**, 533 (1972).
[2] R. Kristoffersen and H. I. Andersson, J. Fluid Mech. **256**, 163 (1993).
[3] U. Piomelli and J. Liu, Phys. Fluids **7**, 839 (1995).
[4] K. Hiwatashi, P. H. Alfredsson, N. Tilmark, and M. Nagata, Phys. Fluids **19**, 048103 (2007).
[5] C. Dong, J. C. McWilliams, and A. F. Shchepetkin, J. Phys. Oceanogr. **37**, 962 (2007)
[6] G. Perret, A. Stegner, M. Farge, and T. Pichon, Phys. Fluids **18**, 036603 (2006).
[7] D. R. Caldwell and J. N. Mourn, Rev. Geophys. **33**, 1385 (1995).
[8] G. R. Mamatsashvili, V. S. Avsarkisov, G. D. Chagelishvili, R. G. Chanishvili, and M. V. Kalashnik, J. Atmos. Sci. **67**, 2972 (2010).
[9] F. G. Jacobitz, S. Sarkar, and C. W. Van Atta, J. Fluid Mech. **342**, 231 (1997).
[10] B. M. Johnson and C. F. Gammie, Astrophys. J. **626**, 978 (2005).
[11] S. A. Balbus and J. F. Hawley, Rev. Mod. Phys. **70**, 1 (1998).
[12] J. M. Lee, J. Kim, and P. Moin, J. Fluid Mech. **216**, 561 (1990).
[13] P. Bradshaw, J. Fluid Mech. **36**, 177 (1969).
[14] D. J. Tritton, J. Fluid Mech., **241**, 503 (1992).
[15] A. Salhi and C. Cambon, J. Fluid Mech. **347**, 171 (1997).
[16] A. Salhi, Theoret. Comp. Fluid Dyn. **15**, 339 (2002).
[17] A. Salhi and C. Cambon, Phys. Rev. E **81**, 026302 (2010).
[18] G. K. Batchelor and I. Proudman, Quantum J. Mech. Appl. Math. **7**, 83 (1954).
[19] H. K. Moffatt, in *Colloquium on Atmospheric Turbulence and Radio Wave Propagation*, edited by A. M. Yaglom and V. I. Tatarski (Nauka, Moscow, 1967), p. 139.
[20] W. Horton, J.-H. Kim, G. D. Chagelishvili, J. C. Bowman, and J. G. Lominadze, Phys. Rev. E **81**, 066304 (2010).
[21] P. Sagaut and C. Cambon, *Homogeneous Turbulence Dynamics* (Cambridge University Press, New York, 2008).
[22] R. S. Rogallo, NASA TM 81315, 1981 (unpublished).
[23] G. Brethouwer, J. Fluid Mech. **542**, 305 (2005).
[24] F. G. Jacobitz, L. Liechtenstein, K. Schneider, and M. Farge, Phys. Fluids **20**, 045103 (2008).
[25] F. G. Jacobitz, K. Schneider, W. J. T. Bos, and M. Farge, Phys. Fluids **22**, 085101 (2010).
[26] S. C. Kassinos, W. C. Reynolds, and M. M. Rogers, J. Fluid Mech. **428**, 213 (2001).
[27] C. Cambon, L. Danaila, F. S. Godeferd, and J. F. Scott, J. Turbul. **14**, 121 (2013).
[28] S. Oughton, K.-H. Rädler, and W. H. Matthaeus, Phys. Rev. E **56**, 2875 (1997).
[29] G. I. Taylor, Proc. R. Soc. London, Ser. A, **151**, 421 (1935).
[30] H. P. Robertson, Proc. Cambridge Philos. Soc. **36**, 209 (1940).
[31] Lord Rayleigh, *Scientific Papers 1*, Vol. 474 (Cambridge University Press, Cambridge, UK, 1880).
[32] A. A. Townsend, J. Fluid Mech. **41**, 13 (1970).
[33] Lord Kelvin, Philos. Mag. **23**, 459 (1887).
[34] C. Lamriben, P. P. Cortet, and F. Moisy, Phys. Rev. Lett. **107**, 024503 (2011).
[35] S. Corrsin, NACA RM 58B11, 1958 (unpublished).
[36] O. Zeman, Phys. Fluids **6**, 3221 (1994).
[37] L. Jacquin, O. Leuchter, C. Cambon, and J. Mathieu, J. Fluid Mech. **220**, 1 (1990).
[38] Y. Morinishi, K. Nakabayashi, and S. K. Ren, Phys. Fluids **13**, 2912 (2001).
[39] A. A. Townsend, *The Structure of Turbulent Shear Flow*, 2nd ed. (Cambridge University Press, Cambridge, UK, 1976).
[40] C. Cambon and L. Jacquin, J. Fluid Mech. **202**, 295 (1989).

[41] C. Cambon and R. Rubinstein, Phys. Fluids **18**, 085106 (2006).
[42] F. G. Jacobitz, K. Schneider, W. J. T. Bos, and M. Farge, Phys. Rev. E **84**, 056319 (2011).
[43] F. G. Jacobitz, K. Schneider, W. J. T. Bos, and M. Farge, J. Turbul. **13**, N35 (2012).
[44] R. Marino, P. D. Mininni, D. Rosenberg, and A. Pouquet, Phys. Rev. E **87**, 033016 (2013).
[45] A. Salhi and C. Cambon, Phys. Fluids **19**, 055102 (2007).
[46] C. Cambon, N.-N. Mansour, and F. S. Godeferd, J. Fluid Mech. **337**, 303 (1997).
[47] C. Cambon, J.-P. Benoit, L. Shao, and L. Jacquin, J. Fluid Mech. **278**, 175 (1994).
[48] F. S. Godeferd, C. Cambon, and S. Leblanc, J. Fluid Mech. **449**, 1 (2001).